Preprint Title	Nanomechanics of few-layer materials: do individual layers slide upon folding?
Authors	Ronaldo J. C. Batista, Rafael F. Dias, Ana P. M. Barboza, Alan B. de Oliveira, Taise M. Manhabosco, Thiago R. Gomes-Silva, Andreij C. Gadellha, Cassiano Rabelo, Luiz G. L. Cançado, Ado Jorio, Hélio Chacham and Bernardo R. A. Neves
Publication Date	03 Aug 2020
Article Type	Full Research Paper
Supporting Information File 1	SuppInf.zip; 1.4 MB
ORCID® iDs	Ronaldo J. C. Batista - https://orcid.org/0000-0002-7471-4968; Ana P. M. Barboza - https://orcid.org/0000-0002-1807-971X; Taise M. Manhabosco - https://orcid.org/0000-0002-4255-5763; Cassiano Rabelo - https://orcid.org/0000-0003-0488-2242; Ado Jorio - https://orcid.org/0000-0002-5978-2735; Bernardo R. A. Neves - https://orcid.org/0000-0003-0464-4754

Nanomechanics of few-layer materials: do individual layers slide upon folding?

Ronaldo J. C. Batista*[1], Rafael F. Dias[2], Ana P. M. Barboza[1], Alan B. de Oliveira[1], Taise M. Manhabosco[1], Thiago R. Gomes-Silva[1], Matheus J. S. Matos[1], Andreij C. Gadelha[3], Cassiano Rabelo[3], Luiz G. L. Cançado[3], Ado Jorio[3], Hélio Chacham[3] and Bernardo R. A. Neves[3]

Address: [1]Departamento de Física, Universidade Federal de Ouro Preto, 35400-000, Ouro Preto, MG, Brazil; [2]Departamento de Física, Universidade Federal de Viçosa, 36570-000, Viçosa, MG, Brazil and [3]Departamento de Física, Universidade Federal de Minas Gerais, 30123-970 Belo Horizonte, MG, Brazil

Email: Ronaldo J. C. Batista - batista.rjc@ufop.edu.br

* Corresponding author

Abstract

Folds naturally appear on nanometrically thin (also called 2D) materials after exfoliation, eventually creating folded edges across the resulting flakes. In the present work, we investigate the adhesion and flexural properties of single and multilayered 2D materials upon folding. This is accomplished by measuring and modeling mechanical properties of folded edges, which allow the experimental determination of the scaling for the bending stiffness (κ) of a multilayered 2D material with its number of layers (n). In the case of talc, we obtain $\kappa \propto n^3$ for $n \geq 5$, establishing that there is no interlayer sliding upon folding, at least in this thickness range. Such a result, if applicable to other materials, would imply that layers in folds might be either compressed (at the inner part of the fold) or stretched (at its outer part), leading to changes in their vibrational properties relative to a flat flake. This hypothesis was confirmed by near-field tip-enhanced Raman spectroscopy of a multilayer graphene fold.

Keywords

atomic force microscopy (AFM); Raman spectroscopy; nanostructured materials; analytical methods; molecular dynamics (MD)

Introduction

Layered materials such as graphite, talc, and transition metal dichalcogenides, held together by strong covalent bonds within layers and by relatively weak van der Waals interlayer interactions, have been the primary source of 2D materials [1]. Such 2D materials depict unusual mechanical properties associated with their flexural properties [2-7]. For instance, 2D materials, unlike 3D materials, can bend over themselves to form folds [4-7], whose curvature radii are functions of the ratio between the interlayer adhesion energy (α) and the layer bending stiffness (κ) [4]. Uncertainties in measured values of α can be large, experimental values of α for graphite ranging from 0.12 up to 0.72 have been reported N/m [8-15]. Regarding the bending stiffness κ, experimental values have been obtained through radial deformations [16], lattice dynamics [17], deformations of suspended layers [2,5], and bubbles profiles[18]. A recent and interesting issue regarding the bending stiffness is its dependence on the thickness or the number of layers of the 2D material [18].

The quantification and understanding of the structural/dynamic response of multilayered 2D materials upon bending is also an important issue regarding technological applications, such as flexible reinforcements for brittle biomedical implants Mota et al.[19] and ultralight resonators suited as transducers of extremely small force or mass changes Will et al.[20]. It is important to emphasize that the quality factor of the resonators depends on its maximum resonant frequency, which is intrinsically related to the flexural properties of the employed 2D material. These properties strongly depend on the in-plane movement of individual layers upon bending, which can also generate heat and, therefore, reduce the performance of those devices.

In this work, we present a method to obtain interlayer adhesion energies and the bending stiffness of 2D materials by experimentally probing the mechanical response of folded edges to deformation. A folded edge is defined as an edge region of the 2D material where it folds over itself during the

exfoliation process. Our method is based on AFM measurements of the geometry and mechanical response of folded edges, and on the fitting of the experimental data by an analytical continuum model parameterized solely by α, κ, and the total thickness d of the 2D folded material. The applicability of the analytical model is corroborated by comparison with classical molecular dynamics simulations. Because folds naturally occur in flakes of varying thickness, corresponding to multilayers with a different number of primitive layers, the proposed method provides a direct way to investigate the scaling of the bending stiffness of 2D materials with flake thickness (or, equivalently, with the number of layers). In the case of talc, we obtain $\kappa \propto h^3$ for materials thicker than five layers, establishing that there is no interlayer sliding upon folding, at least in this thickness range. Such result implies that layers in folds might be either compressed or stretched, leading to changes in their vibrational properties relative to a flat flake, which was confirmed by near-field tip-enhanced Raman spectroscopy of multilayer graphene folds.

Results and Discussion

A 2D folded material deposited on a substrate presents a cross-section geometry similar to that indicated in Fig. 1 (see, for instance, Wang et al [18] and references therein for electron microscope images). Fig. 1(a) shows an AFM image of a talc flake (green shades) with approximately 10 layers, which was exfoliated onto a Si oxide substrate (blue shades). During the exfoliation/deposition processes, such a talc flake folded back and forth over itself, creating a well-defined folded stripe, shown in yellow shades. Fig. 1(b) shows a 3D-perspective zoom of the dashed rectangle region in Fig. 1(a). The red dotted line schematically indicates the back-and-forth folding process which yielded such double-edged folded stripe. Some morphological parameters of a fold can be readily determined from the AFM images, such as its maximum height H, its total thickness d, and its layer thickness h (see the inset in Fig. 1(c) for parameter definition). Fig. 1(c) shows the measured values of two of those parameters, $R_0 = (H - h)/2$ and the flake thickness h for nine talc folds. The measured values of thickness h, from 1.2 nm to 30.0 nm, indicate that the measured folds involve materials from monolayer talc to $\approx$ 30-layer talc. The corresponding values of the radius R_0 span

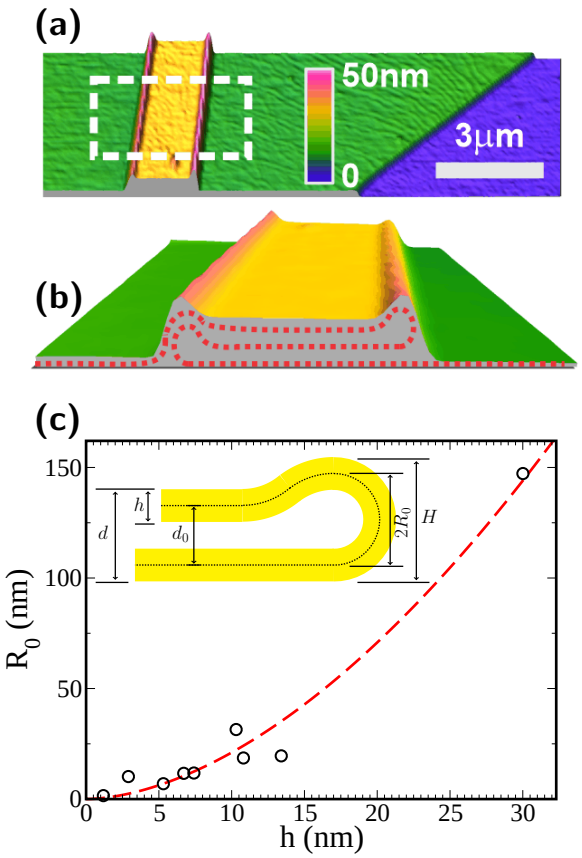

Figure 1: (a) AFM image of a double-folded edge in a talc flake (green-yellow shades) with ≈ 10 layers deposited on a Si-SiOx substrate (blue shades). (b) Perspective view of the region inside the rectangle shown in (a). The dotted line in (b) is a guide for the eye, indicating the formation of the double-folded edges. (C) Values of R_0 for fold edges in talc flakes whose thickness are between 1 and 30 nm. In red, fitted curve $R_0 = ah^b$, where $b = 1.75$ and $a = 0.38$ ($m^{-0.75}$). the inset shows a schematic drawing of a folded edge showing the relevant measured quantities (d, h and H). $R_0 = (H - h)/2$ and $d_0 = d - h$, are parameters for the proposed continuous model.

from 2.15 nm to 162 nm, that is, an increase of two orders of magnitude. The figure also shows a fitted curve $R_0 = ah^b$, where $b = 1.75$ and and $a = 0.38$ ($m^{-0.75}$).

To obtain κ (bending stiffness) and α (adhesion energy) from the AFM data, we propose a continuum variational model (see Supporting Information: Deposited folded edges) for the folded edges with the geometry depicted in Fig. 2. This figure shows both cross-section geometries for folded edges in graphene monolayer, panel (a), and in three-layered graphene, panel (b), obtained through MD simulations (details about MD simulations are found in Supplementary Information). As can be seen in Fig. 2 (a), the model geometry consists of a sequence of straight lines and circular arcs

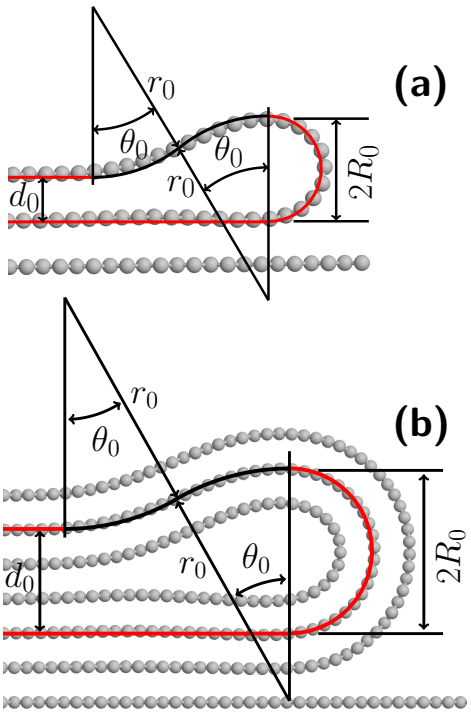

Figure 2: Figure 2. Gray circles: carbon atom positions in cross-sections of folded edges in graphene monolayer, panel (a), and in three-layered graphene, panel (b), as obtained through MD simulations. In both panels the red and black lines that superimpose the atomic positions depict the geometry of folded edges within our variational model, which consists of a sequence of straight lines and circular arcs with radii: R_0 (red arcs) and r_0 (black arcs). In panel (a), the values of R_0 and r_0 are obtained through our model, Eqs. (1) and (2), using experimental values of d_0, κ and α. In panel (b), R_0 and r_0 are obtained through MD simulations.

with two possible radii: the external radius R_0 (red arcs) and the radius r_0 of a half-soliton-like region (black arcs). Within our model, the concave up and the concave down arcs of half-soliton-like region always have the same radius and length. Therefore, the model lines must pass in the middle of the flake for folded edges in flakes more than one atom thick, as it is shown in the inset of Fig. 1 (c) and in Fig. 2 (b) for the three-layered folded edge. The panels of Fig. 2 show that the model geometry describes very well the morphology of folded edges in flakes with different thicknesses (the model lines nearly superimpose atomic positions in both panels of Fig. 2). Within this model, mathematical relations between the geometrical parameters (R_0, r_0, and d_0), and the adhesion (α) and flexural (κ) properties can be obtained variationally. The variational procedure within the model consists of the minimization of an energy functional that contains two terms: the curva-

ture energy $E_c = \int \kappa/(2R^2)dS$ where R is the local curvature radius and κ is the bending stiffness, and the adhesion energy $E_a = \alpha S_a$, where S_a is the contact area and α is the adhesion energy per the unit area between the 2D material and the precursor substrate. As a result of the variational procedure, we obtain (see Supporting Information):

$$r_0 = \sqrt{\frac{3}{2}\frac{\kappa}{\alpha}} \tag{1}$$

and

$$3\pi - \frac{3\pi}{2R_0^2}\left(\frac{\kappa}{\alpha}\right) + \frac{8}{\sqrt{2R_0 - d}}\left(\frac{3}{2}\frac{\kappa}{\alpha}\right)^{1/4} = 0. \tag{2}$$

Equations (1) and (2) can be used to determine either the folded edge geometry from the properties of the 2D material (κ/α and thickness) or vice-versa. In the particular case of the folded edge in graphene monolayer shown in 2 (a), we use literature values for $\alpha = 0.37$ N/m [14] and $\kappa = 0.231$ aJ [21] to determine r_0 and R_0. On the other hand, in the case of the folded edge in three-layered graphene, we use the values of $R_0 = 0.81$ nm and $d_0 = 1.01$ nm from MD simulations to obtain $\sqrt{\kappa/\alpha} = 1.88$ nm. Considering α the same for both graphene folded edges, we thus found $\kappa = 1.3$ aJ for three-layered graphene, which is roughly 6 times the value reported for the graphene monolayer ($\kappa = 0.231$ aJ). Thus, MD results indicate that the scaling of κ with the number of layers in multi-layered graphene is non-linear. The scaling of κ in a real 2D material will be discussed below.

Equation 2 allows us to obtain the ratio κ/α for talc folds through measured values for R_0 and d_0. Fig. 3 shows the quantity $Q = \sqrt{h\alpha/\kappa} = \sqrt{h}/\sqrt{\kappa/\alpha}$ versus $1/h$ for the nine measured talc samples. h is a directly measured quantity (see Fig.1), and $\sqrt{\frac{\kappa}{\alpha}}$ as we mentioned earlier, is obtained from Eq. 2. Assuming that α is constant for a given material, the behavior of Q as a function of h, $Q(h)$, will be solely dependent on the behavior of κ as a function of h. In the limit of thick materials, we would expect that adjacent layers do not slide relative to each other upon an elastic bend-

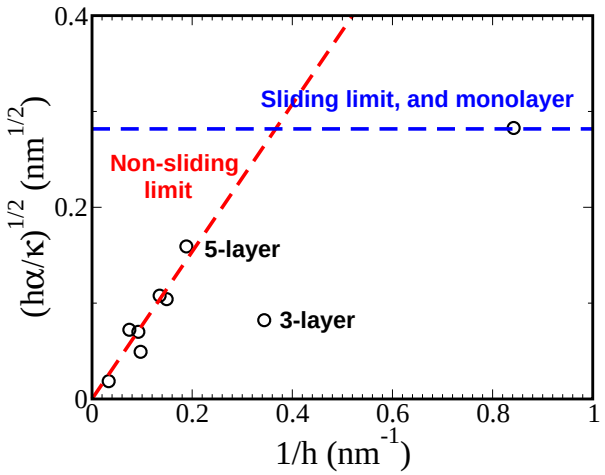

Figure 3: $\sqrt{h\alpha/\kappa} = \sqrt{h}/\sqrt{\kappa/\alpha}$ versus $1/h$ for the nine measured talc samples. h is a directly measured quantity (see Fig. 1), and $\sqrt{\kappa/\alpha}$ is obtained from Eq. 2 with the measured values of R_0 and h. The red and blue lines correspond to the ideal non-sliding ($\kappa \propto h^3$) and the sliding ($\kappa \propto h$) limits, respectively. The values for the thinnest samples (monolayer, 3-layer and 5-layer talc) are explicitly indicated.

ing deformation. In this non-sliding limit, we expect that $\kappa \propto h^3$, as predicted by the classical Euler-Bernoulli beam theory. In another limit, which we will call a sliding limit, we will assume the possibility that adjacent layers freely slide upon bending deformations. In this limit, which implicitly includes the monolayer case, we obtain $\kappa \propto h$. Both limits have been recently considered in the analysis of experimental profiles of bubbles in 2D materials [18]. In our present analysis, the functional form of Q leads to two asymptotic limits as a function of $1/h$: $Q \propto 1/h$ in the non-sliding limit, and Q =constant in the sliding limit. Both limits are indicated in Fig. 3 as red and blue lines, fitted respectively to the seven thickest samples and the monolayer sample. Therefore, Fig. 3 indicates that individual layers of multilayer talc with at least more than 4 layers do not slide upon folding. In contrast, we were not able to observe any sample behaving according to the proposed sliding limit, besides the (trivial, by definition) monolayer case. The 4- and 2-layer cases were absent in our samples, and the 3-layer case shows an anomalous behavior relative to the other samples, being much stiffer than expected: it might, for instance, possess a distinct morphology. From the above, we conclude that thick enough talc flakes behave like rigid objects, without interlayer sliding. Therefore, upon fold formation, the layers at the inner part of the fold will have a compressive in-plane strain, and those at the outer part will have an extensive (tensile) in-plane

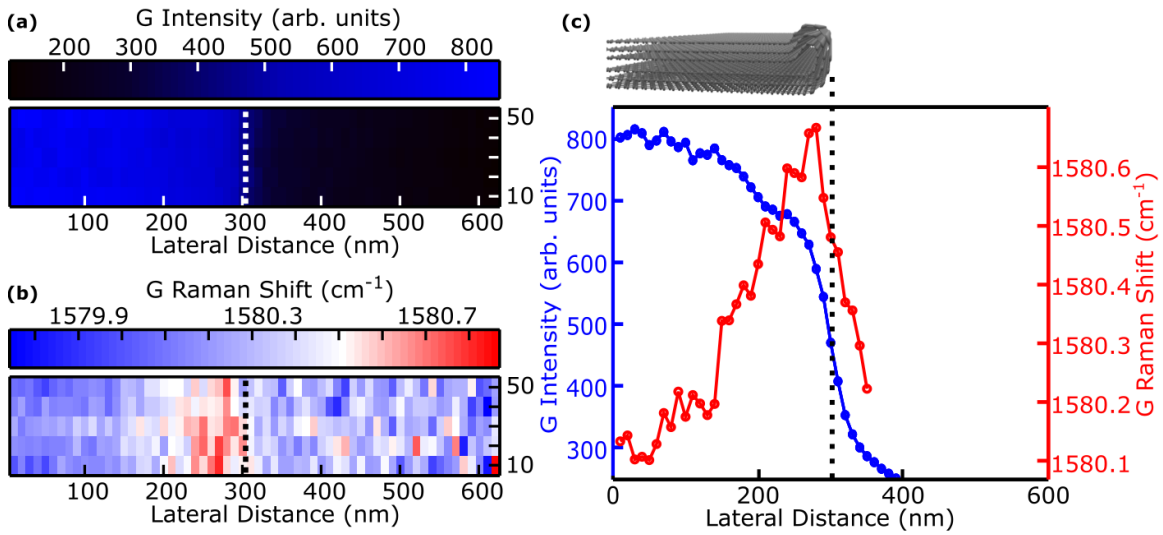

Figure 4: (a) Near-field Raman image of the intensity of the G peak as a function of the lateral distance, where the blue and dark blue regions correspond to the folded graphene flake and the substrate, respectively, and the dashed white line marks the location of the edge of the fold. (b) Map of relative Raman shift, where blue corresponds to lower frequencies and red to higher frequencies. (c) Intensity (blue) and relative Raman shift (red) of the G peak as a function of the lateral distance.

strain. Such strains could modify the vibrational properties of a fold relative to the (flat) bulk of the flake and it should be universal to any 2D material, and not restricted to talc. This hypothesis was investigated employing a near-field tip-enhanced Raman spectroscopy (TERS) setup [22,23], which can probe strain variations across the edge of a folded graphene flake(Fig. 4). Panel (a) shows a near-field Raman map of the intensity of the G peak, where the blue and dark blue regions correspond to the folded graphene flake and the substrate, respectively, and the dashed white line marks the location of the edge of the fold. Fig. 4 (b) shows a map of the Raman shift for the same fold, it exhibits displacements towards high frequencies near the edge of the fold. To detect such displacements clearly, we average the horizontal lines in Fig. 4 (a) and (b), and depict the result in Fig. 4(c), where we plot the relative Raman shift (red curve) and intensity (blue curve) of the G peak as a function of the lateral distance. The vertical dotted black line in this panel marks the position of the folded edge, where a change in the position of the G peak is also observed. It has been previously shown that compressive strain in graphene causes displacements in the G peak toward high frequencies [24]. For the folded few-layer graphene edge, both the outermost (tensile) and innermost (compressive) regions contribute to the Raman spectrum. However, the innermost layers

have smaller curvature radii compared to the outermost, which would give a net compressive contribution to the Raman. Therefore, the observed positive displacement in the G mode is consistent with our hypothesis that the outermost and innermost graphene regions in a multi-layered graphene folded edge tend to be stretched and compressed, respectively.

We have so far addressed the ratio κ/α of talc folds, obtained from Eq. (2) with the measured values of R_0 and d for uncompressed folds. As already discussed, the quantity κ/α allowed us to verify a prevalence of the non-sliding behavior, independently verified by Raman measurements. One might, however, be also interested in obtaining the absolute values of κ and α from the AFM. In fact, to the best of our knowledge, no experimental measurement of α for talc has been reported so far. Now we will show that it is possible to obtain the value of α from AFM force curve measurements on folded edges. According to our model (see Supporting Information: Compressed folded edges), when a spherical probe compresses a folded edge, the mechanical response is given by:

$$\begin{aligned}\frac{F(D)}{\sqrt{2R_s}} = &\left[(\alpha_p-\alpha)\sqrt{\frac{2R_0-d}{16r_0}} - (\alpha+\alpha_p)\frac{\pi}{2}\right]\sqrt{D} \\ &+\frac{2r_0^2\pi\alpha}{3}\left[\frac{\arctan\sqrt{\frac{D}{2R_0-D}}}{(2R_0-D)^{3/2}} + \frac{\sqrt{D}}{(2R_0-D)2R_0}\right] \\ &+\left[\frac{(\alpha_p-\alpha)(2R_0-d-D)}{8\sqrt{r_0}} + \frac{4\alpha\sqrt{r_0}}{3}\right]\ln\left(\frac{\sqrt{2R_0-d}+\sqrt{D}}{\sqrt{2R_0-d}-\sqrt{D}}\right).\end{aligned} \tag{3}$$

where D is the deformation caused by the probe, R_s is the probe radius, and α_p is the adhesion energy per unit area between the 2D sample and the probe. Despite its length, the Eq. (3) contains only two adjustable parameters - α and α_p - as the AFM height profiles provide R_0 and d, while r_0 can be obtained through Eqs. (1) and (2). Panel (a) of Figure 5 shows the fit of Eq. (3) to AFM force vs deformation measurements on a 5.3 nm thick talc fold. The obtained value of $\alpha = 0.60$ N/m is consistent with the few theoretical results available (0.30 N/m [25] and 0.98 N/m [26]). Also, the obtained value of $\alpha_p = 0.42$ N/m indicates that the interaction between talc and the silicon probe is smaller than the interaction between talc layers. To combine data of several force

curve measurements in a single graph, we plotted the re-scaled force $F/\sqrt{2R_s r_0}$ as a function of the strain $D/(2R_0 - d)$ as shown in Fig. 5(b). The red curve in this figure represents our model (see Supporting Information equation S13). The resulting values of $\alpha = 0.62$ N/m and $\alpha_p = 0.40$ N/m are similar to those obtained in the fitting of panel (a), showing consistency between those results.

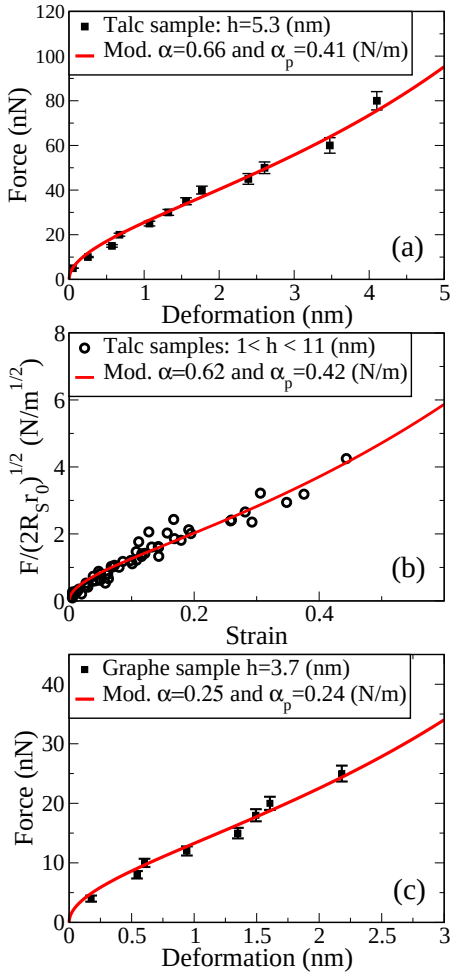

Figure 5: **(a)**: best fit of Eq. 3 to measured AFM forces and deformations on a 5.3 nm thick talc fold. **(b)**: best fit of Eq. (3) to forces and deformations in folded edges of several talc flakes, with thicknesses of 1.2, 2.9, 5.3, 6.7, 7.4 and 10.9 nm. The vertical axis is the re-scaled force, $F/\sqrt{2R_s r_0}$, and the horizontal axis is the strain $S = D/(2R_0 - d)$ (see Supporting Information). **(c)**: best fit of Eq. (3) to AFM measurements on a fold in a 11-layer-thick graphene flake.

Unlike talc, there are several results in the literature on the interlayer adhesion energy of graphene [10-15], providing good references to evaluate the α predicted by of our model. Figure 5(c) shows the best fit of Eq. (3) to AFM measurements for a 11-layer-thick graphene fold. To fit the exper-

imental data, we used R_0 = 4.5 nm and d = 5.25 nm obtained from the height profile and r_0 = 11.7 nm obtained through Eqs. (1) and (2). The obtained value of α = 0.25 N/m is within the range of values obtained experimentally (from 0.12 up to 0.72 N/m [8-15]). It is worth mentioning that our result (α=0.25 N/m) compares well with other direct experimental determination of α (0.27 N/m [12] and 0.37 N/m [14]) in which layers of graphene in highly oriented pyrolytic graphite were mechanically manipulated using a probe. Besides, the value obtained for the interaction between graphite and the silicon probe (α_p=0.24 N/m) is consistent with the values reported in the literature [27,28] (0.28 and 0.37 N/m).

Conclusions

In summary, we have shown that it is possible to obtain the interlayer adhesion energy and the bending stiffness of 2D layered materials by fitting results of AFM force curves on naturally occurring folded edges to an expression predicted by a simple model for those edges. The obtained interlayer adhesion energy for graphene (0.25 N/m) and talc (0.62 N/m) are in good agreement with recent experimental results [12,14], and theoretical predictions [25,29], respectively. The proposed method also allows the investigation of bending stiffness dependence with the flake thickness. For talc flakes with a thickness equal or larger than 5.3 nm, we obtained a scaling relation ($\kappa \propto h^3$) that is consistent with the Euler-Bernoulli beam theory. Such a result implies that, in this non-sliding regime, layers in 2D materials folds are either stretched (at the outer part of the fold) or compressed (at the inner part). This was confirmed by near-field Raman spectroscopy. Even though it is applied here to homo-layers, the present methodology could also, bring invaluable insights about the interlayer interaction in the growing field of 2D materials hetero-layers, probing the mechanical properties of typical interfaces such as graphene/hBN, graphene/TMDs, hBN/TMDS or any other technologically relevant two-dimensional heterostructure.

Supporting Information

Supporting information features the theoretical models for deposited and compressed folded edges,

the experimental methods (including sample preparations, SPM characterization and Near-field tip-enhaced Raman spectroscopy) and the MD simulations computational details.

Supporting Information File 1:

File Name: S1.pdf

File Format: PDF

Title: Models, experimental part and computational details

Funding

This work was supported by the Conselho Nacional de Desenvolvimento Científico e Tecnológico (CNPq); Coordenação de Aperfeiçoamento de Pessoal de Nível Superior (CAPES); Fundação de Amparo à Pesquisa do Estado de Minas Gerais (FAPEMIG); the Brazilian Institute of Science and Technology (INCT) in Carbon Nanomaterials; and Universidade Federal de Ouro Preto (UFOP-Grant Custeio).

References

1. Novoselov, K. S.; Geim, A. K.; Morozov, S. V.; Jiang, D.; Zhang, Y.; Dubonos, S. V.; Grigorieva, I. V.; Firsov, A. A. *Science* **2004**, *306* (5696), 666–669.

2. Chacham, H.; Barboza, A. P. M.; de Oliveira, A. B.; de Oliveira, C. K.; Batista, R. J. C.; Neves, B. R. A. *Nanotechnology* **2018**, *29* (9), 095704.

3. Ferrari, G. A.; de Oliveira, A. B.; Silvestre, I.; Matos, M. J. S.; Batista, R. J. C.; Fernandes, T. F. D.; Meireles, L. M.; Eliel, G. S. N.; Chacham, H.; Neves, B. R. A.; Lacerda, R. G. *ACS Nano* **2018**, *12* (5), 4312–4320.

4. de Lima, A. L.; Muessnich, L. A. M.; Manhabosco, T. M.; Chacham, H.; Batista, R. J. C.; de Oliveira, A. B. *Nanotechnology* **2015**, *26* (4), 045707–045714.

5. Blees, M. K.; Barnard, A. W.; Rose, P. A.; Roberts, S. P.; McGill, K. L.; Huang, P. Y.; Ruyack, A. R.; Kevek, J. W.; Kobrin, B.; Muller, D. A.; McEuen, P. L. *Nature* **2015**, *524* (7564), 204–207.

6. Oliveira, C. K.; Gomes, E. F. A.; Prado, M. C.; Alencar, T. V.; Nascimento, R.; Malard, L. M.; Batista, R. J. C.; de Oliveira, A. B.; Chacham, H.; de Paula, A. M.; Neves, B. R. A. *Nano Research* **2015**, *8* (5), 1680–1688.

7. Barboza, A. P. M.; Chacham, H.; Oliveira, C. K.; Fernandes, T. F. D.; Ferreira, E. H. M.; Archanjo, B. S.; Batista, R. J. C.; de Oliveira, A. B.; Neves, B. R. A. *Nano Letters* **2012**, *12* (5), 2313–2317.

8. Girifalco, L. A. *Ph.D. Thesis*; University of Cincinnati, 1954.

9. Girifalco, L. A.; Lad, R. A. *The Journal of Chemical Physics* **1956**, *25* (4), 693–697.

10. Benedict, L.; Chopra, N.; Cohen, M.; Zettl, A.; Louie, S.; Crespi, V. *Chemical Physics Letters* **1998**, *286* (5-6), 490–496.

11. Zacharia, R.; Ulbricht, H.; Hertel, T. *Physical Review B* **2004**, *69* (15), 155406.

12. Liu, Z.; Liu, J. Z.; Cheng, Y.; Li, Z.; Wang, L.; Zheng, Q. *Physical Review B* **2012**, *85* (20), 205418.

13. Roenbeck, M. R.; Wei, X.; Beese, A. M.; Naraghi, M.; Furmanchuk, A.; Paci, J. T.; Schatz, G. C.; Espinosa, H. D. *ACS Nano* **2014**, *8* (1), 124–138.

14. Wang, W.; Dai, S.; Li, X.; Yang, J.; Srolovitz, D. J.; Zheng, Q. *Nature Communications* **2015**, *6*, 7853.

15. van Engers, C. D.; Cousens, N. E. A.; Babenko, V.; Britton, J.; Zappone, B.; Grobert, N.; Perkin, S. *Nano Letters* **2017**, *17* (6), 3815–3821.

16. Barboza, A. P. M.; Chacham, H.; Neves, B. R. A. *Physical Review Letters* **2009**, *102* (2), 025501.

17. Nicklow, R.; Wakabayashi, N.; Smith, H. G. *Phys. Rev. B* **1972**, *5*, 4951–4962.

18. Wang, G.; Dai, Z.; Xiao, J.; Feng, S.; Weng, C.; Liu, L.; Xu, Z.; Huang, R.; Zhang, Z. *Phys. Rev. Lett.* **2019**, *123*, 116101.

19. Mota, L. M.; Nicomendes, D. N. N.; Barboza, A. P. M.; Ramos, S. L. L. d. M.; Vasconcellos, R. V.; Medrado, N. V.; Alvarenga, É. C.; Machado, G.; Juste, K. R.; Vasconcelos, C. K. d.; Righi, A.; Manhabosco, S. M.; Resende, R. R.; Batista, R. J. C.; Soares, J. d. S.; Manhabosco, T. *Surface and Coatings Technology* **2020**, *397*, 126005.

20. Will, M.; Hamer, M.; Müller, M.; Noury, A.; Weber, P.; Bachtold, A.; Gorbachev, R. V.; Stampfer, C.; Güttinger, J. *Nano Letters* **2017**, *17* (10), 5950–5955.

21. Wei, Y.; Wang, B.; Wu, J.; Yang, R.; Dunn, M. L. *Nano Letters* **2013**, *13* (1), 26–30.

22. Vasconcelos, T. L.; Archanjo, B. S.; Oliveira, B. S.; Valaski, R.; Cordeiro, R. C.; Medeiros, H. G.; Rabelo, C.; Ribeiro, A.; Ercius, P.; Achete, C. A.; Jorio, A.; Cançado, L. G. *Advanced Optical Materials* **2018**, *6* (20), 1800528.

23. Araujo, P. T.; Barbosa Neto, N. M.; Chacham, H.; Carara, S. S.; Soares, J. S.; Souza, A. D.; Cancado, L. G.; de Oliveira, A. B.; Batista, R. J. C.; Joselevich, E.; Dresselhaus, M. S.; Jorio, A. *NANO LETTERS* **2012**, *12* (8), 4110–4116.

24. Frank, O.; Tsoukleri, G.; Parthenios, J.; Papagelis, K.; Riaz, I.; Jalil, R.; Novoselov, K. S.; Galiotis, C. *ACS Nano* **2010**, *4* (6), 3131–3138.

25. Alencar, A. B.; Barboza, A. P. M.; Archanjo, B. S.; Chacham, H.; Neves, B. R. A. *2D Materials* **2015**, *2* (1), 015004.

26. Ward, W.; Phillips, J. M. *Surface Science* **1971**, *25* (2), 379 –384.

27. Na, S. R.; Suk, J. W.; Ruoff, R. S.; Huang, R.; Liechti, K. M. *ACS Nano* **2014**, *8* (11), 11234–11242.

28. Gao, X.; Yu, X.; Li, B.; Fan, S.; Li, C. *Advanced Materials Interfaces* **2017**, *4* (9), 1601023.

29. Han, E.; Yu, J.; Annevelink, E.; Son, J.; Kang, D. A.; Watanabe, K.; Taniguchi, T.; Ertekin, E.; Huang, P. Y.; van der Zande, A. M. *Nature Materials* **2020**, *19* (3), 305–309.